

# RSC Advances



This is an *Accepted Manuscript*, which has been through the Royal Society of Chemistry peer review process and has been accepted for publication.

*Accepted Manuscripts* are published online shortly after acceptance, before technical editing, formatting and proof reading. Using this free service, authors can make their results available to the community, in citable form, before we publish the edited article. This *Accepted Manuscript* will be replaced by the edited, formatted and paginated article as soon as this is available.

You can find more information about *Accepted Manuscripts* in the [Information for Authors](#).

Please note that technical editing may introduce minor changes to the text and/or graphics, which may alter content. The journal's standard [Terms & Conditions](#) and the [Ethical guidelines](#) still apply. In no event shall the Royal Society of Chemistry be held responsible for any errors or omissions in this *Accepted Manuscript* or any consequences arising from the use of any information it contains.

## Inhibition studies of *Helicobacter pylori* urease with Schiff base copper(II) complexes

Zhonglu You<sup>a,\*</sup>, Mingyang Liu<sup>a</sup>, Cunfang Wang<sup>b</sup>, Guihua Sheng<sup>b</sup>, Xinlu Zhao<sup>a</sup>,  
Dan Qu<sup>a</sup>, Fang Niu<sup>a</sup>

<sup>a</sup> Department of Chemistry and Chemical Engineering, Liaoning Normal University, Dalian 116029, P. R. China

<sup>b</sup> School of Life Sciences, Shandong University of Technology, Zibo 255049, P. R. China

### Abstract

Nine new copper(II) complexes derived from various Schiff bases were prepared. They are  $[\text{Cu}_2\text{Br}_2(\text{L}^1)_2]$  (**1**),  $[\text{Cu}(\text{L}^2)_2] \cdot 2\text{NO}_3 \cdot 2\text{CH}_3\text{OH}$  (**2**),  $[\text{Cu}(\text{L}^3)_2] \cdot 2\text{Br}$  (**3**),  $[\text{Cu}(\text{L}^4)_2]$  (**4**),  $[\text{Cu}_2\text{Cl}_4(\text{L}^2)_2]$  (**5**),  $[\text{Cu}_2\text{Cl}_2(\text{L}^5)_2]$  (**6**),  $[\text{CuL}^6(\text{NCS})]$  (**7**),  $[\text{CuClL}^6] \cdot \text{CH}_3\text{OH}$  (**8**), and  $[\text{Cu}_2(\text{L}^7)_2]$  (**9**), where  $\text{L}^1$  is the monoanionic form of 2-chloro-*N'*-(4-diethylamino-2-hydroxybenzylidene)benzohydrazide ( $\text{HL}^1$ ),  $\text{L}^2$  is the zwitterionic form of 4-methyl-2-((3-morpholinopropylimino)methyl)phenol ( $\text{L}^2$ ),  $\text{L}^3$  is the zwitterionic form of 2-bromo-4-chloro-6-((2-(2-hydroxyethylamino)ethylimino)methyl)phenol ( $\text{L}^3$ ),  $\text{L}^4$  is the monoanionic form of 2-bromo-4-chloro-6-((cyclopentylimino)methyl)phenol ( $\text{HL}^4$ ),  $\text{L}^5$  is the monoanionic form of 2-((cyclopropylimino)methyl)-4-methylphenol ( $\text{HL}^5$ ),  $\text{L}^6$  is the monoanionic form of

\* Corresponding author. Zhonglu You, Department of Chemistry and Chemical Engineering, Liaoning Normal University, Dalian 116029, P. R. China. Tel.: +8641182156711. E-mail address: youzhonglu@163.com

4-methyl-2-((pyridin-2-ylmethylimino)methyl)phenol (HL<sup>6</sup>), and L<sup>7</sup> is the dianionic form of *N,N'*-bis(5-methylsalicylidene)-1,4-diiminobutane (H<sub>2</sub>L<sup>7</sup>). The complexes were characterized by infrared and UV-Vis spectra, and single crystal X-ray diffraction. The Cu atoms in complex **1** display square pyramidal coordination, in complex **5** display trigonal bipyramidal coordination, in complex **9** show tetrahedrally distorted square planar coordination, and in the remaining complexes display square planar coordination. Complexes **2**, **3**, **5**, **7** and **8** show effective urease inhibitory activities, with IC<sub>50</sub> values of  $0.37 \pm 1.22$ ,  $0.21 \pm 0.97$ ,  $0.03 \pm 0.78$ ,  $0.39 \pm 0.58$  and  $0.76 \pm 0.95$   $\mu\text{M}$ , respectively. Molecular docking study of the complexes with *Helicobacter pylori* urease was performed. Complex **5** has the most effective activity against urease, with a mixed competitive inhibition mechanism. The complex interacts with the nickel atom of the urease active center, and with the remaining parts of the complex molecule block the entrance of the urease active pocket.

*Keywords:* Aroylhydrazone; Copper complex; Crystal structure; Urease inhibition; Molecular docking

## Introduction

Urease (urea amidohydrolase; E.C.3.5.1.5) occurs throughout the animal, plant kingdoms, and bacteria. Many microorganisms use this enzyme to provide a source of nitrogen for growth, and it plays an important role in plant nitrogen metabolism during the germination process [1-3]. The presence of urease activity in soils is exploited in the widespread agricultural practice of urea-based fertilizer application for enhancing crop yields [4-7]. Unfortunately, excessive levels of soil urease can degrade the fertilizer urea too rapidly, and result in phytopathic effects and loss of

volatilized ammonia [8]. In addition, this enzyme is regarded as a virulent factor in human and animal infections of the urinary and gastrointestinal tracts. It may cause urolithiasis, pyelonephritis, chronic gastritis, duodenal ulcer, gastric ulcer, and even gastric cancer [9].

Control of the activity of urease through the use of inhibitors could counteract the negative effects [10]. To date, four major classes of urease inhibitors have been extensively investigated, namely hydroxamic acids [11-13], phosphoroamide compounds [14], boric and boronic acids [15,16], and heavy metal salts [17,18]. It has been found that the inhibitor mechanism of action and the kinetics of inhibition for bacterial urease and jack bean urease are similar. Therefore, urease from any source, be it bacterial or plant, can be used as a model system for inhibition studies, and results would be equally applicable for any system or field of application [19].

Metal complexes have been known as interesting enzyme inhibitors [20]. From the point of structural and coordination chemistry, many organic urease inhibitors are excellent ligands, which can coordinate to inorganic urease inhibitors. The complexes bearing both organic and inorganic components may possess higher urease inhibitory activities than their precursors. In recent years, we have reported a number of metal complexes with urease inhibitory activities [21-25]. Among the compounds, copper(II) complexes have the highest urease inhibitory activities. Li and coworkers have reported some Schiff base copper(II) complexes with potent urease inhibitory activities [26,27]. However, study on urease inhibition by metal complexes is still in its infancy. In particular, the relationship between structures and urease inhibitory activities is not clear. In this paper, a series of new copper(II) complexes,  $[\text{Cu}_2\text{Br}_2(\text{L}^1)_2]$  (**1**),  $[\text{Cu}(\text{L}^2)_2] \cdot 2\text{NO}_3 \cdot 2\text{CH}_3\text{OH}$  (**2**),  $[\text{Cu}(\text{L}^3)_2] \cdot 2\text{Br}$  (**3**),  $[\text{Cu}(\text{L}^4)_2]$  (**4**),  $[\text{Cu}_2\text{Cl}_4(\text{L}^2)_2]$  (**5**),  $[\text{Cu}_2\text{Cl}_2(\text{L}^5)_2]$  (**6**),  $[\text{CuL}^6(\text{NCS})]$  (**7**),  $[\text{CuClL}^6] \cdot \text{CH}_3\text{OH}$  (**8**), and  $[\text{Cu}_2(\text{L}^7)_2]$  (**9**), where

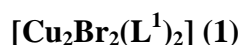
$L^1$  is the monoanionic form of 2-chloro-*N'*-(4-diethylamino-2-hydroxybenzylidene)benzohydrazide ( $HL^1$ ),  $L^2$  is the zwitterionic form of 4-methyl-2-((3-morpholinopropylimino)methyl)phenol ( $L^2$ ),  $L^3$  is the zwitterionic form of 2-bromo-4-chloro-6-((2-(2-hydroxyethylamino)ethylimino)methyl)phenol ( $L^3$ ),  $L^4$  is the monoanionic form of 2-bromo-4-chloro-6-((cyclopentylimino)methyl)phenol ( $HL^4$ ),  $L^5$  is the monoanionic form of 2-((cyclopropylimino)methyl)-4-methylphenol ( $HL^5$ ),  $L^6$  is the monoanionic form of 4-methyl-2-((pyridin-2-ylmethylimino)methyl)phenol ( $HL^6$ ), and  $L^7$  is the dianionic form of *N,N'*-bis(5-methylsalicylidene)-1,4-diiminobutane ( $H_2L^7$ ), were synthesized and structurally characterized. The urease inhibitory activity of the complexes was investigated both from experimental and molecular docking analysis.

## Experimental

### Materials and measurements

Starting materials, reagents and solvents were purchased from commercial suppliers with AR grade, and used without purification. *Helicobacter pylori* urease was purchased from Sigma-Aldrich Co. (St. Louis, MO, USA). The Schiff bases were prepared according to the literature method [28]. Elemental analyses were performed on a Perkin-Elmer 240C elemental analyzer. IR spectra were recorded on a Jasco FT/IR-4000 spectrometer as KBr pellets in the 4000–400  $\text{cm}^{-1}$  region. UV-Vis spectra were recorded on a Perkin-Elmer Lambda 900 spectrometer. The urease inhibitory activity was measured on a Bio-Tek Synergy HT microplate reader. Single crystal structures were determined by Bruker D8 Venture single crystal diffraction.

### Synthesis of the complexes



The Schiff base HL<sup>1</sup> (1.0 mmol, 0.345 g) was dissolved in methanol (15 mL), to which was added dropwise CuBr<sub>2</sub> (1.0 mmol, 0.223 g) dissolved in methanol (10 mL). The mixture was magnetic stirred for 10 min at room temperature, and filtered. The filtrate was kept in air for a few days, to form crystals suitable for single crystal X-ray diffraction. The crystals were isolated, washed three times with cold methanol and dried in a vacuum desiccator containing anhydrous CaCl<sub>2</sub>. Yield: 193 mg (40%). Characteristic IR data (KBr, cm<sup>-1</sup>): 3243 (NH), 1600 (CH=N). UV-Vis data [methanol, λ/nm (ε/L·mol<sup>-1</sup>·cm<sup>-1</sup>): 269 (4,450), 392 (15,270), 650 (130). Anal. Calcd for C<sub>16</sub>H<sub>13</sub>CuN<sub>3</sub>O<sub>2</sub>S: C, 44.3; H, 3.9; N, 8.6. Found: C, 44.1; H, 4.0; N, 8.7%. *A<sub>M</sub>* (10<sup>-3</sup> M in acetonitrile): 15 Ω<sup>-1</sup> cm<sup>2</sup> mol<sup>-1</sup>.

#### **[Cu(L<sup>2</sup>)<sub>2</sub>]·2NO<sub>3</sub>·2CH<sub>3</sub>OH (2)**

The Schiff base L<sup>2</sup> (1.0 mmol, 0.262 g) was dissolved in methanol (15 mL), to which was added dropwise Cu(NO<sub>3</sub>)<sub>2</sub> (1.0 mmol, 0.242 g) dissolved in methanol (10 mL). The mixture was magnetic stirred for 10 min at room temperature, and filtered. The filtrate was kept in air for a few days, to form crystals suitable for single crystal X-ray diffraction. The crystals were isolated, washed three times with cold methanol and dried in a vacuum desiccator containing anhydrous CaCl<sub>2</sub>. Yield: 127 mg (33%). Characteristic IR data (KBr, cm<sup>-1</sup>): 3378 (OH), 3223 (NH), 1612 (CH=N), 1377 (NO<sub>3</sub>), 853 (NO<sub>3</sub>). UV-Vis data [methanol, λ/nm (ε/L·mol<sup>-1</sup>·cm<sup>-1</sup>): 273 (12,328), 378 (4,330), 660 (160). Anal. Calcd for C<sub>32</sub>H<sub>52</sub>CuN<sub>6</sub>O<sub>12</sub>: C, 49.5; H, 6.8; N, 10.8. Found: C, 49.7; H, 6.7; N, 11.0%. *A<sub>M</sub>* (10<sup>-3</sup> M in acetonitrile): 220 Ω<sup>-1</sup> cm<sup>2</sup> mol<sup>-1</sup>.

#### **[Cu(L<sup>3</sup>)<sub>2</sub>]·2Br (3)**

The Schiff base L<sup>3</sup> (1.0 mmol, 0.322 g) was dissolved in methanol (15 mL), to which was added dropwise CuBr<sub>2</sub> (1.0 mmol, 0.223 g) dissolved in methanol (10 mL). The mixture was magnetic stirred for 10 min at room temperature, and filtered. The filtrate

was kept in air for a few days, to form crystals suitable for single crystal X-ray diffraction. The crystals were isolated, washed three times with cold methanol and dried in a vacuum desiccator containing anhydrous  $\text{CaCl}_2$ . Yield: 175 mg (40%). Characteristic IR data (KBr,  $\text{cm}^{-1}$ ): 3430 (OH), 3184 (NH), 1633 (CH=N). UV-Vis data [methanol,  $\lambda/\text{nm}$  ( $\epsilon/\text{L}\cdot\text{mol}^{-1}\cdot\text{cm}^{-1}$ ): 270 (14,130), 383 (6,580), 615 (225). Anal. Calcd for  $\text{C}_{22}\text{H}_{28}\text{Br}_4\text{Cl}_2\text{CuN}_4\text{O}_4$ : C, 30.5; H, 3.3; N, 6.5. Found: C, 30.2; H, 3.1; N, 6.4%.  $A_M$  ( $10^{-3}$  M in acetonitrile):  $240 \Omega^{-1} \text{cm}^2 \text{mol}^{-1}$ .

#### [Cu(L<sup>4</sup>)<sub>2</sub>] (4)

The Schiff base HL<sup>4</sup> (1.0 mmol, 0.302 g) was dissolved in methanol (15 mL), to which was added dropwise  $\text{CuBr}_2$  (1.0 mmol, 0.223 g) dissolved in methanol (10 mL). The mixture was magnetic stirred for 10 min at room temperature, and filtered. The filtrate was kept in air for a few days, to form crystals suitable for single crystal X-ray diffraction. The crystals were isolated, washed three times with cold methanol and dried in a vacuum desiccator containing anhydrous  $\text{CaCl}_2$ . Yield: 113 mg (34%). Characteristic IR data (KBr,  $\text{cm}^{-1}$ ): 1621 (CH=N). UV-Vis data [methanol,  $\lambda/\text{nm}$  ( $\epsilon/\text{L}\cdot\text{mol}^{-1}\cdot\text{cm}^{-1}$ ): 270 (12,990), 375 (7,140). Anal. Calcd for  $\text{C}_{24}\text{H}_{24}\text{Br}_2\text{Cl}_2\text{CuN}_2\text{O}_2$ : C, 43.2; H, 3.6; N, 4.2. Found: C, 43.3; H, 3.7; N, 4.0%.  $A_M$  ( $10^{-3}$  M in acetonitrile):  $25 \Omega^{-1} \text{cm}^2 \text{mol}^{-1}$ .

#### [Cu<sub>2</sub>Cl<sub>4</sub>(L<sup>2</sup>)<sub>2</sub>] (5)

The Schiff base L<sup>2</sup> (1.0 mmol, 0.262 g) was dissolved in methanol (15 mL), to which was added dropwise  $\text{CuCl}_2$  (1.0 mmol, 0.170 g) dissolved in methanol (10 mL). The mixture was magnetic stirred for 10 min at room temperature, and filtered. The filtrate was kept in air for a few days, to form crystals suitable for single crystal X-ray diffraction. The crystals were isolated, washed three times with cold methanol and dried in a vacuum desiccator containing anhydrous  $\text{CaCl}_2$ . Yield: 212 mg (53%).

Characteristic IR data (KBr,  $\text{cm}^{-1}$ ): 3264 (NH), 1637s (CH=N). UV-Vis data [methanol,  $\lambda/\text{nm}$  ( $\epsilon/\text{L}\cdot\text{mol}^{-1}\cdot\text{cm}^{-1}$ ): 275 (13,550), 326 (3,980), 380 (4,110), 570 (135). Anal. Calcd for  $\text{C}_{30}\text{H}_{44}\text{Cl}_4\text{Cu}_2\text{N}_4\text{O}_4$ : C, 45.4; H, 5.6; N, 7.1. Found: C, 45.3; H, 5.7; N, 7.0%.  $A_M$  ( $10^{-3}$  M in acetonitrile):  $17 \Omega^{-1} \text{cm}^2 \text{mol}^{-1}$ .

#### **[Cu<sub>2</sub>Cl<sub>2</sub>(L<sup>5</sup>)<sub>2</sub>] (6)**

The Schiff base HL<sup>5</sup> (1.0 mmol, 0.175 g) was dissolved in methanol (15 mL), to which was added dropwise CuCl<sub>2</sub> (1.0 mmol, 0.170 g) dissolved in methanol (10 mL). The mixture was magnetic stirred for 10 min at room temperature, and filtered. The filtrate was kept in air for a few days, to form crystals suitable for single crystal X-ray diffraction. The crystals were isolated, washed three times with cold methanol and dried in a vacuum desiccator containing anhydrous CaCl<sub>2</sub>. Yield: 115 mg (42%). Characteristic IR data (KBr,  $\text{cm}^{-1}$ ): 1621 (CH=N). UV-Vis data [methanol,  $\lambda/\text{nm}$  ( $\epsilon/\text{L}\cdot\text{mol}^{-1}\cdot\text{cm}^{-1}$ ): 271 (11,620), 320 (5,420), 380 (2,255). Anal. Calcd for  $\text{C}_{22}\text{H}_{24}\text{Cl}_2\text{Cu}_2\text{N}_2\text{O}_2$ : C, 48.4; H, 4.4; N, 5.1. Found: C, 48.1; H, 4.6; N, 5.3%.  $A_M$  ( $10^{-3}$  M in acetonitrile):  $28 \Omega^{-1} \text{cm}^2 \text{mol}^{-1}$ .

#### **[CuL<sup>7</sup>(NCS)] (7)**

The Schiff base HL<sup>7</sup> (1.0 mmol, 0.226 g) and ammonium thiocyanate (1.0 mmol, 0.076 g) were dissolved in methanol (15 mL), to which was added dropwise Cu(CH<sub>3</sub>COO)<sub>2</sub> (1.0 mmol, 0.199 g) dissolved in methanol (10 mL). The mixture was magnetic stirred for 10 min at room temperature, and filtered. The filtrate was kept in air for a few days, to form crystals suitable for single crystal X-ray diffraction. The crystals were isolated, washed three times with cold methanol and dried in a vacuum desiccator containing anhydrous CaCl<sub>2</sub>. Yield: 155 mg (45%). Characteristic IR data (KBr,  $\text{cm}^{-1}$ ): 2098 (NCS), 1628 (CH=N). UV-Vis data [methanol,  $\lambda/\text{nm}$  ( $\epsilon/\text{L}\cdot\text{mol}^{-1}\cdot\text{cm}^{-1}$ ): 275 (12,780), 388 (3,990), 600 (172). Anal. Calcd for

$C_{15}H_{13}CuN_3OS$ : C, 51.9; H, 3.8; N, 12.1. Found: C, 51.7; H, 3.7; N, 11.9%.  $A_M$  ( $10^{-3}$  M in acetonitrile):  $40 \Omega^{-1} \text{ cm}^2 \text{ mol}^{-1}$ .

### **[CuCIL<sup>6</sup>] $\cdot$ CH<sub>3</sub>OH (8)**

The Schiff base HL<sup>6</sup> (1.0 mmol, 0.226 g) was dissolved in methanol (15 mL), to which was added dropwise CuCl<sub>2</sub> (1.0 mmol, 0.170 g) dissolved in methanol (10 mL). The mixture was magnetic stirred for 10 min at room temperature, and filtered. The filtrate was kept in air for a few days, to form crystals suitable for single crystal X-ray diffraction. The crystals were isolated, washed three times with cold methanol and dried in a vacuum desiccator containing anhydrous CaCl<sub>2</sub>. Yield: 113 mg (32%). Characteristic IR data (KBr,  $\text{cm}^{-1}$ ): 1629 (CH=N). UV-Vis data [methanol,  $\lambda/\text{nm}$  ( $\epsilon/\text{L}\cdot\text{mol}^{-1}\cdot\text{cm}^{-1}$ ): 275 (12,890), 310 (3,470), 390 (3,986), 490 (510), 630 (170). Anal. Calcd for  $C_{15}H_{17}ClCuN_2O_2$ : C, 50.6; H, 4.8; N, 7.9. Found: C, 50.3; H, 4.9; N, 7.9%.  $A_M$  ( $10^{-3}$  M in acetonitrile):  $36 \Omega^{-1} \text{ cm}^2 \text{ mol}^{-1}$ .

### **[Cu<sub>2</sub>(L<sup>7</sup>)<sub>2</sub>] (9)**

The Schiff base H<sub>2</sub>L<sup>7</sup> (1.0 mmol, 0.324 g) was dissolved in methanol (15 mL), to which was added dropwise Cu(CH<sub>3</sub>COO)<sub>2</sub> (1.0 mmol, 0.199 g) dissolved in methanol (10 mL). The mixture was magnetic stirred for 10 min at room temperature, and filtered. The filtrate was kept in air for a few days, to form crystals suitable for single crystal X-ray diffraction. The crystals were isolated, washed three times with cold methanol and dried in a vacuum desiccator containing anhydrous CaCl<sub>2</sub>. Yield: 89 mg (23%). Characteristic IR data (KBr,  $\text{cm}^{-1}$ ): 1621 (CH=N). UV-Vis data [methanol,  $\lambda/\text{nm}$  ( $\epsilon/\text{L}\cdot\text{mol}^{-1}\cdot\text{cm}^{-1}$ ): 276 (11,490), 380 (4,620), 620 (120). Anal. Calcd for  $C_{40}H_{44}Cu_2N_4O_4$ : C, 62.2; H, 5.7; N, 7.3. Found: C, 62.3; H, 5.9; N, 7.1%.  $A_M$  ( $10^{-3}$  M in acetonitrile):  $10 \Omega^{-1} \text{ cm}^2 \text{ mol}^{-1}$ .

### **X-ray crystallography**

Diffraction intensities for the complexes were collected at 298(2) K using a Bruker D8 Venture diffractometer with MoK $\alpha$  radiation ( $\lambda = 0.71073$  Å). The collected data were reduced with SAINT [29], and multi-scan absorption correction was performed using SADABS [30]. Structures of the complexes were solved by direct methods and refined against  $F^2$  by full-matrix least-squares method using SHELXTL [31]. All of the non-hydrogen atoms were refined anisotropically. The amino H atoms in **1**, **2** and **5** were located from difference Fourier maps and refined isotropically, with N–H distances restrained to 0.90(1) Å. The remaining hydrogen atoms were placed in calculated positions and constrained to ride on their parent atoms. Crystallographic data for the complexes are summarized in Tables 1a–1c. Selected bond lengths and angles are given in Table 2.

#### **Urease inhibitory activity assay**

*Helicobacter pylori* (ATCC 43504; American Type Culture Collection, Manassas, VA) was grown in brucella broth supplemented with 10% heat-inactivated horse serum for 24 h at 37 °C under microaerobic condition (5% O<sub>2</sub>, 10% CO<sub>2</sub>, and 85% N<sub>2</sub>). The method of preparation of *Helicobacter pylori* urease by Mao [32] was followed. Briefly, broth cultures (50 mL,  $2.0 \times 10^8$  CFU mL<sup>-1</sup>) were centrifuged (5000 g, 4 °C) to collect the bacteria, and after washing twice with phosphate-buffered saline (pH 7.4), the *Helicobacter pylori* precipitation was stored at –80 °C. While the *Helicobacter pylori* was returned to room temperature, and mixed with 3 mL of distilled water and protease inhibitors, sonication was performed for 60 s. Following centrifugation (15,000 g, 4 °C), the supernatant was desalted through SephadexG–25 column (PD–10 columns, Amersham–Pharmacia Biotech, Uppsala, Sweden). The resultant crude urease solution was added to an equal volume of glycerol and stored at 4 °C until use in the experiment. The mixture, containing 25  $\mu$ L (4U) of *Helicobacter*

*pylori* urease and 25  $\mu\text{L}$  of the test compound, was pre-incubated for 3 h at room temperature in a 96-well assay plate. Urease activity was determined by measuring ammonia production using the indophenol method as described by Weatherburn [33].

#### **Inhibition kinetic study**

The maximum velocity ( $v_{\text{max}}$ ) values were determined by means of Lineweaver–Burk plots, using initial velocities obtained over substrate concentrations of 25.00, 12.50, 6.25, and 3.125 mM, respectively. Inhibitory constant ( $K_i$ ) value was calculated from the Dixon plot. Alternatively,  $K_i$  value was determined from abscissa of the plots of slopes vs. different concentrations of the complex, in which slope was obtained from the Lineweaver–Burk lines [34].

#### **Docking study**

Molecular docking study of the complexes into the 3D X-ray structure of the *Helicobacter pylori* urease (entry 1E9Y in the Protein Data Bank) was carried out by using the AutoDock 4.0 software as implemented through the graphical user interface AutoDockTools (ADT 1.5.2). The graphical user interface AutoDockTools was employed to setup the enzymes: all hydrogens were added, Gasteiger charges were calculated and nonpolar hydrogens were merged to carbon atoms. The Ni initial parameters are set as  $r = 1.170 \text{ \AA}$ ,  $q = +2.0$ , and *van der* Waals well depth of  $0.100 \text{ kcal}\cdot\text{mol}^{-1}$  [35]. The 3D structures of the ligand molecules were saved in pdb format with the aid of the program ChemBio3D. The resulting files were saved as pdbqt format.

The AutoDockTools was used to generate the docking input files. In the docking, grid box sizes of  $76 \times 64 \times 88$  for **1**,  $84 \times 72 \times 94$  for **2**,  $84 \times 100 \times 68$  for **3**,  $72 \times 66 \times 58$  for **4**,  $40 \times 58 \times 58$  for **5**,  $42 \times 52 \times 56$  for **6**,  $88 \times 72 \times 70$  for **7**,  $54 \times 64 \times 58$  for **8**, and  $58 \times 60 \times 48$  for **9**, respectively, points in  $x$ ,  $y$ , and  $z$  directions were built, the

maps were centered on the original ligand molecule (HAE) in the catalytic site of the protein. A grid spacing of 0.375 Å and a distances-dependent function of the dielectric constant were used for the calculation of the energetic map. 100 runs were generated by using Lamarckian genetic algorithm searches. Default settings were used with an initial population of 50 randomly placed individuals, a maximum number of  $2.5 \times 10^6$  energy evaluations, and a maximum number of  $2.7 \times 10^4$  generations. A mutation rate of 0.02 and a crossover rate of 0.8 were chosen. The results of the most favorable free energy of binding were selected as the resultant complex structures.

## Results and discussion

### Chemistry

The copper complexes were readily prepared by the reaction of equimolar quantities of Schiff bases, copper salts, and/or secondary ligands (NCS) in methanol. Single crystals of the complexes were obtained by slow evaporation of the methanolic solution of the complexes. The aroylhydrazone Schiff base ligands in complex **1** adopt *keto* form. The Schiff base ligands in complexes **2**, **3** and **5** adopt zwitterionic form. The Schiff base ligands in the remaining complexes adopt monoanionic form. The complexes are stable in air at room temperature. Molar conductivity of complexes **1**, **4**, **5**, **6**, **7**, **8** and **9** measured in methanol at concentration of  $10^{-3}$  M are in the range of  $10\text{-}40 \Omega^{-1} \text{ cm}^2 \text{ mol}^{-1}$ , indicating the non-electrolytic nature of them in such solution [36]. Molar conductivity of complexes **2** and **3** measured in methanol at concentration of  $10^{-3}$  M are in the range of  $220\text{-}240 \Omega^{-1} \text{ cm}^2 \text{ mol}^{-1}$ , indicating the 1:2 electrolytic nature of them in such solution [36].

### Structure description of the complexes

#### Structure description of **1**

Molecular structure of complex **1** is shown in Figure 1. The complex is a

phenolate-bridged dinuclear copper(II) compound, with a crystallographic inversion center located at the midpoint of the two Cu atoms. The Cu···Cu separation is 3.004(1) Å. The Cu atoms in the complex are in square pyramidal geometry, with the phenolate O, imino N and carbonyl O atoms of the aroylhydrazone Schiff base ligands located at the basal plane, and with the Br atom located at the apical position. The Cu atoms deviate from the least-squares planes defined by the four basal donor atoms by 0.289(1) Å. The coordinate bond lengths in the complex are comparable to those observed in copper(II) complexes with aroylhydrazone Schiff bases [37,38]. The distortion of the square pyramidal geometry can be observed from the deviation of the coordinate bond angles from the ideal square pyramid (Table 2), which are caused by the strain created from the four-membered chelate ring Cu1-O1-Cu1A-O1A and the five-membered chelate ring Cu1-N1-N2-C8-O2. The dihedral angle between the two benzene rings of the ligand is 61.4(5)°.

In the crystal structure of the complex, molecules are linked through intermolecular hydrogen bonds (Table 3), to form 1D chains along the *a* axis (Figure S1).

#### **Structure description of complexes 2, 3 and 4**

Molecular structures of complexes **2**, **3** and **4** are shown in Figures 2, 3 and 4, respectively. All the complexes possess crystallographic inversion center symmetry. Complex **2** contains a mononuclear copper(II) complex cation, two nitrate anions, and two methanol molecules of crystallization. Complex **3** contains a mononuclear copper(II) complex cation, and two bromide anions. The Cu atoms in the complexes are coordinated by two phenolate O and two imino N atoms from two Schiff base ligands, forming square planar geometry. The Cu–O and Cu–N bond lengths in the complexes are comparable to each other, and also similar to those observed in copper(II) complexes with Schiff bases [39,40]. The crystal structures of complexes **2**

and **3** are stabilized by hydrogen bonds (Table 3, Figures S2 and S3).

### Structure description of complex **5**

Molecular structure of complex **5** is shown in Figure 5. The complex is a phenolate-bridged dinuclear copper(II) compound, with a crystallographic inversion center located at the midpoint of the two Cu atoms. The Cu...Cu separation is 3.167(1) Å. The Cu atoms in the complex are in trigonal bipyramidal geometry, with the phenolate O atom of one Schiff base ligand, and two Cl atoms located at the basal plane, and with one N atom of the Schiff base ligand, and the phenolate O atom of the other Schiff base ligand located at the apical position. The Cu atoms deviate from the least-squares planes defined by the three basal donor atoms by 0.052(1) Å. The coordinate bond lengths in the complex are comparable to those observed in copper(II) complexes with Schiff bases [41,42]. The distortion of the trigonal bipyramidal geometry can be observed from the deviation of the coordinate bond angles from the ideal trigonal bipyramid (Table 2), which are caused by the strain created from the four-membered chelate ring Cu1-O1-Cu1A-O1A. The coordination configuration is proved by the structural index  $\tau$  [43] which represents the relative amount of trigonality (square pyramid,  $\tau = 0$ ; trigonal bipyramid,  $\tau = 1$ );  $\tau = (\beta - \alpha)/60^\circ$ ,  $\alpha$  and  $\beta$  being the two largest angles around the central atom. The value of  $\tau$  in the complex is 0.55. Crystal structure of the complex is stabilized by hydrogen bonds (Table 3, Figure S4).

### Structure description of complex **6**

Molecular structure of complex **6** is shown in Figure 6. The complex is a phenolate-bridged dinuclear copper(II) compound, with a crystallographic inversion center located at the midpoint of the two Cu atoms. The Cu...Cu separation is 3.066(1) Å. The Cu atoms in the complex are coordinated by phenolate O and imino N atoms

from the Schiff base ligands, and Cl atoms, forming tetrahedrally distorted square planar geometry. The Cu atoms deviate from the least-squares planes defined by the four donor atoms by 0.061(1) Å. The coordinate bond lengths in the complex are comparable to those observed in the above complexes with square planar geometry. The distortion of the square planar geometry can be observed from the *cis* and *trans* bond angles, which are in the range 76.3(2)–102.2(2)° and 150.7(2)–152.1(3)°, respectively.

### Structure description of complexes **7** and **8**

Molecular structures of complexes **7** and **8** are shown in Figures 7 and 8, respectively. The complexes are very similar except for the secondary ligands, *viz.* NCS for **7**, and Cl for **8**. In addition, complex **8** comprises a methanol molecule of crystallization. The Cu atoms in the complexes are coordinated by phenolate O, imino N and pyridine N atoms of the Schiff base ligand, and one secondary ligand, forming square planar geometry. The coordinate bond lengths in both complexes are comparable to each other, and also similar to those observed in the above complexes with square planar geometry. The dihedral angles between the benzene ring and the pyridine ring are 6.0(3)° for **7** and 8.5(4)° for **8**. In the crystal structure of complex **8**, the methanol molecules are linked to the copper complex molecules through intermolecular hydrogen bonds (Table 3, Figure S5).

### Structure description of complex **9**

Molecular structure of complex **9** is shown in Figure 9. The complex is a dinuclear copper(II) compound, which contains a 14-membered ring. The Cu atoms in the complex are coordinated by two phenolate O and two imino N atoms from two Schiff base ligands, forming tetrahedrally distorted square planar geometry. The Cu1 and Cu2 atoms deviate from the least-squares planes defined by the four donor atoms by

0.022(1) Å and 0.046(1) Å, respectively. The coordinate bond lengths in the complex are comparable to those observed in the above complexes with square planar geometry. The distortion of the square planar geometry can be observed from the *cis* and *trans* bond angles, which are in the range 92.48(9)–94.89(9)° and 146.99(10)–154.02(10)°, respectively.

### IR and UV-Vis spectra

The medium and broad absorption in the region 3300–3500 cm<sup>-1</sup> in the spectra of complexes **2** and **3** substantiate the presence of O–H groups. The sharp bands indicative of the N–H vibrations of complexes **1**, **2**, **3** and **5** are located at 3180–3270 cm<sup>-1</sup>. The strong absorption bands in the region 1600–1640 cm<sup>-1</sup> for the complexes are assigned to the azomethine  $\nu(\text{C}=\text{N})$  [44]. The intense absorption at 2098 cm<sup>-1</sup> for complex **7** can be assigned to the vibration of the NCS ligands [45]. The bands indicative of the nitrate anions are observed at 1377 and 853 cm<sup>-1</sup>.

Electronic spectra of the complexes were recorded in acetonitrile with concentration of 10<sup>-5</sup> M. The complexes displayed strong bands centered at about 270 nm, which can be assigned to the intraligand  $\pi$ – $\pi^*$  transition of the benzene rings. The charge transfer LMCT bands are located in the range 370–390 nm. The medium absorption at 326 nm for complex **5**, 320 nm for complex **6**, and 310 nm for complex **8** are assigned to another type of LMCT bands. The spectra showed weak and broad *d*–*d* electronic transitions in the range 560–660 nm, which are assigned to  ${}^2E_{g(D)} \rightarrow {}^2T_{2g(D)}$  [46]. The broadness of the bands is due to the ligand field and the Jahn-Teller effects.

### Pharmacology study

The percent inhibition of the complexes at concentration of 100  $\mu\text{M}$  on *Helicobacter pylori* urease is summarized in Table 4. Complexes **2**, **3**, **5**, **7** and **8** show strong urease

inhibitory activity with  $IC_{50}$  values of  $0.37 \pm 1.22$ ,  $0.21 \pm 0.97$ ,  $0.03 \pm 0.78$ ,  $0.39 \pm 0.58$ , and  $0.76 \pm 0.95 \mu\text{M}$ , respectively. Complex **4** show medium activity with  $IC_{50}$  value of  $80.1 \pm 3.2 \mu\text{M}$ . However, complexes **1**, **6** and **9** have very weak or no activity on urease. As a comparison, acetohydroxamic acid (AHA) was used as a reference with the percent inhibition of  $84.3 \pm 3.9$ , and with  $IC_{50}$  value of  $37.2 \pm 4.0 \mu\text{M}$ . Copper perchlorate can inhibit urease activity, with  $IC_{50}$  value of  $8.8 \pm 1.4 \mu\text{M}$ . Complexes **2**, **3**, **5**, **7** and **8** have stronger activities than the metal complexes reported in the literature [39, 47-52] (Table 4).

#### **Kinetic study of the urease inhibitory activity by complex 5**

Complex **5** has the most effective urease inhibitory activity. Thus, the inhibition mechanism of the complex was studied with Lineweaver-Burk plots (Figure 10a). The type of inhibition was elucidated from analysis of Lineweaver-Burk plots. For Lineweaver-Burk plot, the slope of the resulting line is  $K_m/v_{\text{max}}$ , the  $y$ -intercept is  $1/v_{\text{max}}$ , and the  $x$ -intercept is  $1/K_m$ . The figure shows a series of lines intersect one with another in the third quadrant while the  $y$ -intercept of the plots increased with the increase of the concentration (3.125, 6.25, 12.50, 25.00 mM) of the complex. This illustrated the inhibition of the urease by the complex caused a decrease in  $v_{\text{max}}$  with change of  $K_m$  values, suggesting a mixed-competitive inhibition type. The  $K_i$  value of  $-15.0$  was calculated from the slope of the Lineweaver-Burk plot vs. the concentration of inhibitor (Figure 10b).

#### **Molecular docking study**

Molecular docking study was performed to investigate the binding effects between the molecules of the complexes and the active site of the *Helicobacter pylori* urease. In the X-ray structure available for the native *Helicobacter pylori* urease, two nickel atoms were coordinated by HIS136, HIS138, KCX219, HIS248, HIS274, ASP362 and

water molecules, while in the AHA inhibited urease, the water molecules were replaced by AHA. The binding models of complexes **2**, **3**, **5**, **7** and **8** with the urease were depicted in Figures 11-15, respectively. The binding models of complexes **1**, **4**, **6** and **9** with the urease were depicted in Figures S6-S9, respectively. The results revealed that the molecules of complexes **2**, **3**, **5**, **7** and **8** fit well with the active pocket of the urease, while complexes **1**, **4**, **6** and **9**, due to the large bulk, can not enter the active pocket. This might be the basal principle of the inhibition. Additional interactions have been established in a variety of conformations because of the flexibility of the complex molecules and the amino acid residues of the enzyme. The optimized clusters (100 occurrences each) were ranked by energy level in the best conformation of inhibitor–urease modeled structures, where the docking scores are  $-6.97$  (**1**),  $-7.47$  (**2**),  $-7.85$  (**3**),  $-7.19$  (**4**),  $-7.79$  (**5**),  $-6.51$  (**6**),  $-5.10$  (**7**),  $-5.15$  (**8**), and  $-7.38$  (**9**), respectively. As a comparison, the docking score for the AHA inhibited model is  $-5.01$ . The negative values indicate that the complex molecules bind well with the urease.

The mechanism of urease inhibition was considered to be blockage of the entrance of the urease active pocket and the interaction of the key residue CYS321. It is observed that the Cu atoms of complexes **2**, **3**, **7**, and **8** are involved in the interaction with the residue CYS321, a key residue dedicated to catalytic activity, forming  $\text{Cu}\cdots\text{S}$  bonds with distances of 2.5-3.2 Å. In addition, there are hydrogen bonds and hydrophobic interactions among the complexes and the residues of the urease. Complex **2** forms hydrogen bonds with the residues HIS322 and MET317, and hydrophobic interactions with the residues ALA169, ASN168 and VAL320. Complex **3** forms hydrogen bonds with the residues VAL320, ARG338 and GLU222. Complex **7** forms hydrophobic interactions with the residues HIS322 and ALA365. Complex **8**

forms hydrophobic interactions with the residue MET366. As for complex **5** there is no Cu<sup>II</sup>–S interaction due to the trigonal bipyramidal coordination. The complex forms hydrogen bond with the residue PRG163, and hydrophobic interaction with the residue ALA365. Moreover, the morpholin oxygen of the Schiff base ligand forms interaction with the nickel atom (Ni3001) of the urease active center.

### Conclusion

The present study reports synthesis, characterization and crystal structures of nine new copper(II) complexes with Schiff bases. Complexes **2**, **3**, **5**, **7** and **8** show effective urease inhibitory activities, with IC<sub>50</sub> values of  $0.37 \pm 1.22$ ,  $0.21 \pm 0.97$ ,  $0.03 \pm 0.78$ ,  $0.39 \pm 0.58$  and  $0.76 \pm 0.95$   $\mu\text{M}$ , respectively. Complex **5** has the most effective activity against urease, with a mixed competitive inhibition mechanism. The complex interacts with the nickel atom of the urease active center, and with the remaining parts of the complex molecule block the entrance of the urease active pocket. Molecular docking study indicated that suitable size and conformations of the complexes are required for the inhibition of the urease. The biological evaluation and mechanism study of the compounds reveal that they are prospective urease inhibitors.

### Supplementary data

CCDC 1418882 (**1**), 1418883 (**2**), 1418892 (**3**), 1418904 (**4**), 1418889 (**5**), 1418888 (**6**), 1418897 (**7**), 1418890 (**8**) and 1418891 (**9**) contain the supplementary crystallographic data for this paper. These data can be obtained free of charge *via* <http://www.ccdc.cam.ac.uk/conts/retrieving.html>, or from the Cambridge Crystallographic Data Centre, 12 Union Road, Cambridge CB2 1EZ, UK; fax: (+44) 1223-336-033; or e-mail: [deposit@ccdc.cam.ac.uk](mailto:deposit@ccdc.cam.ac.uk).

### Acknowledgments

This work was financially supported by the Natural Science Foundation of Liaoning Province (Project No. 2015020673), the Program for Liaoning Excellent Talents in University (Project No. LR2014032), and the Undergraduate Training Program for Innovation and Entrepreneurship of Liaoning Province (Project No. 201510165079).

## References

1. S. Cruchaga, B. Lasa, I. Jauregui, C. Gonzalez-Murua, P. M. Aparicio-Tejo and I. Ariz, *Plant Soil*, 2013, **373**, 813.
2. P. A. Karplus, M. A. Pearson and R. P. Hausinger, *Acc. Chem. Res.*, 1997, **30**, 330.
3. J. B. Sumner, *J. Biol. Chem.*, 1926, **69**, 435.
4. L. E. Zonia, N. E. Stebbins, J. C. Polacco, *Plant Physiol*, 1995, **107**, 1097.
5. C. M. Collins and S. E. F. DÓrazio, *Mol. Microbiol.*, 1993, **9**, 907.
6. C. Montecucco and R. Rappuoli, *Nat. Rev. Mol. Cell Biol.*, 2001, **2**, 457.
7. W. Zhengping, O. Van Cleemput, P. Demeyer and L. Baert, *Biol. Fertil. Soils*, 1991, **11**, 41.
8. J. R. Soares, H. Cantarella and M. L. D. Menegale, *Soil Biol. Biochem.*, 2012, **52**, 82.
9. M. Perrais, C. Rousseaux, M. P. Ducourouble, R. Courcol, P. Vincent, N. Jonckheere and I. Van Seuningen, *Gastric Cancer*, 2014, **17**, 235.
10. L. V. Modolo, A. X. de Souza, L. P. Horta, D. P. Araujo and A. de Fatima, *J. Adv. Res.*, 2015, **6**, 35.
11. Z.-P. Xiao, Z.-Y. Peng, J.-J. Dong, R.-C. Deng, X.-D. Wang, H. Ouyang, P. Yang, J. He, Y.-F. Wang and M. Zhu, *Eur. J. Med. Chem.*, 2013, **68**, 212.
12. T. G. Barros, J. S. Williamson, O. A. C. Antunes and E. M. F. Muri, *Lett. Drug Des. Discov.*, 2009, **6**, 186.

13. Zaheer- Ul -Haq, A. Wadood and R. Uddin, *J. Enzyme Inhib. Med. Chem.*, 2009, **24**, 272.
14. K. F. Bronson and A. R. Mosier, *Biol. Fert. Soils*, 1994, **17**, 263.
15. K. R. C. Reddy and A. M. Kayastha, *J. Enzyme Inhib. Med. Chem.*, 2006, **21**, 467.
16. S. Kumar and A. M. Kayastha, *J. Enzyme Inhib. Med. Chem.*, 2010, **25**, 646.
17. W. Zaborska, B. Krajewska and Z. Olech, *J. Enzym. Inhib. Med. Chem.*, 2004, **19**, 65.
18. W. Zaborska, B. Krajewska, M. Leszko and Z. Olech, *J. Mol. Catal. B: Enzym*, 2001, **13**, 103.
19. S. Kumar and A. M. Kayastha, *J. Enzyme Inhib. Med. Chem.*, 2010, **25**, 646.
20. A. Y. Louie and T. J. Meade, *Chem. Rev.*, 1999, **99**, 2711.
21. D. Qu, F. Niu, X. Zhao, K.-X. Yan, Y.-T. Ye, J. Wang, M. Zhang and Z. You, *Bioorg. Med. Chem.*, 2015, **23**, 1944.
22. Z.-L. You, L. Zhang, D.-H. Shi, X.-L. Wang, X.-F. Li and Y.-P. Ma, *Inorg. Chem. Commun.*, 2010, **13**, 996.
23. Z.-L. You, D.-H. Shi, J.-C. Zhang, Y.-P. Ma, C. Wang and K. Li, *Inorg. Chim. Acta*, 2012, **384**, 54.
24. Z.-L. You, Y. Lu, N. Zhang, B.-W. Ding, H. Sun, P. Hou and C. Wang, *Polyhedron*, 2011, **30**, 2186.
25. Z.-L. You, L.-L. Ni, D.-H. Shi and S. Bai, *Eur. J. Med. Chem.*, 2010, **45**, 3196.
26. X.-W. Dong, T.-L. Guo, Y.-G. Li, Y.-M. Cui and Q. Wang, *J. Inorg. Biochem.*, 2013, **127**, 82.
27. Y.-M. Cui, X.-W. Dong, W. Chen, W.-J. Wang, Y.-G. Li and H.-L. Zhu, *J. Enzyme Inhib. Med. Chem.*, 2012, **27**, 528.
28. M. Zhang, D.-M. Xian, H.-H. Li, J.-C. Zhang and Z.-L. You, *Aust. J. Chem.*, 2012,

- 65, 343.
29. Bruker, SMART (Version 5.628) and SAINT (Version 6.02); Bruker AXS: Madison, Wisconsin, USA, 1998.
30. G. M. Sheldrick, SADABS Program for Empirical Absorption Correction of Area Detector; University of Göttingen: Germany, 1996.
31. G. M. Sheldrick, *Acta Crystallogr.*, 2008, **A64**, 112.
32. W.-J. Mao, P.-C. Lv, L. Shi, H.-Q. Li and H.-L. Zhu, *Bioorg. Med. Chem.*, 2009, **17**, 7531.
33. M. W. Weatherburn, *Anal. Chem.*, 1967, **39**, 971.
34. Z. Amtul, M. Rasheed, M. I. Choudhary, R. Supino, K. M. Khan, R. Atta Ur, *Biochem. Biophys. Res. Commun.*, 2004, **319**, 1053.
35. B. Krajewska and W. Zaborska, *Bioorg. Chem.*, 2007, **35**, 355.
36. W. J. Geary, *Coord. Chem. Rev.*, 1971, **7**, 81.
37. L.-M. Wu, H.-B. Teng, X.-C. Feng, X.-B. Ke, Q.-F. Zhu, J.-T. Su, W.-J. Xu and X.-M. Hu, *Cryst. Growth Des.*, 2007, **7**, 1337.
38. M. F. Iskander, T. E. Khalil, R. Werner, W. Haase, I. Svoboda and H. Fuess, *Polyhedron*, 2000, **19**, 1181.
39. W. Chen, Y. G. Li, Y. M. Cui, X. Zhang, H.-L. Zhu and Q.F. Zeng, *Eur. J. Med. Chem.*, 2010, **45**, 4473.
40. R. Kilincarslan, H. Karabiyik, M. Ulusoy, M. Aygun, B. Cetinkaya and O. Buyukgungor, *J. Coord. Chem.*, 2006, **59**, 1649.
41. R. Paschke, S. Liebsch, C. Tschierske, M. A. Oakley and E. Sinn, *Inorg. Chem.*, 2003, **42**, 8230.
42. J. Manzur, A. M. Garcia, A. Vega and A. Ibanez, *Polyhedron*, 2007, **26**, 115.
43. A. W. Addison, T. N. Rao, J. Reedijk, J. van Rijn and G. C. Verschoor, *J. Chem.*

- Soc. Dalton Trans.*, **1984**, 1349.
44. Z.-L. You, M. Zhang and D.-M. Xian, *Dalton Trans.*, 2012, **41**, 2515.
45. Z.-L. You, D.-M. Xian and M. Zhang, *CrystEngComm*, 2012, **14**, 7133.
46. A. A. Alhadi, S. A. Shaker, W. A. Yehye, H. M. Ali and M. A. Abdullah, *Bull. Chem. Soc. Ethiopia*, 2012, **26**, 95.
47. L. Habala, A. Roller, M. Matuska, J. Valentova, A. Rompel and F. Devinsky, *Inorg. Chim. Acta*, 2014, **421**, 423.
48. Y. Gou, M. Yu, Y. Li, Y. Peng and W. Chen, *Inorg. Chim. Acta*, 2013, **404**, 224.
49. H. Zhu, Z.-Z. Wang, B. Qi, T. Huang, H.-L. Zhu, *J. Coord. Chem.*, 2013, **66**, 2980.
50. Y.-P. Xu, Y.-H. Chen, Z.-J. Chen, J. Qin, S.-S. Qian, H.-L. Zhu, *Eur. J. Inorg. Chem.*, 2015, 2076.
51. M. K. Rauf, S. Yaseen, A. Badshah, S. Zaib, R. Arshad, Imtiaz-ud-Din, M. N. Tahir, J. Iqbal, *J. Biol. Inorg. Chem.*, 2015, **20**, 541.
52. X. Dong, Y. Li, Z. Li, Y. Cui, H. Zhu, *J. Inorg. Biochem.*, 2012, **108**, 22.

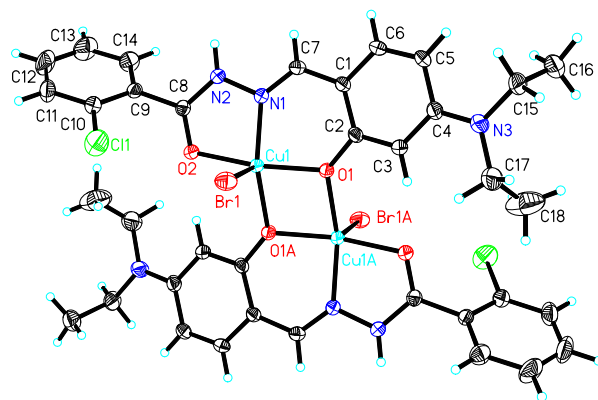


Figure 1. Molecular structure of **1**, showing the atom-numbering scheme. Displacement ellipsoids are drawn at the 30% probability level and H atoms are shown as small spheres of arbitrary radii. Unlabeled atoms or atoms labeled with the suffix A are related to the symmetry position  $1 - x, 1 - y, 2 - z$ .

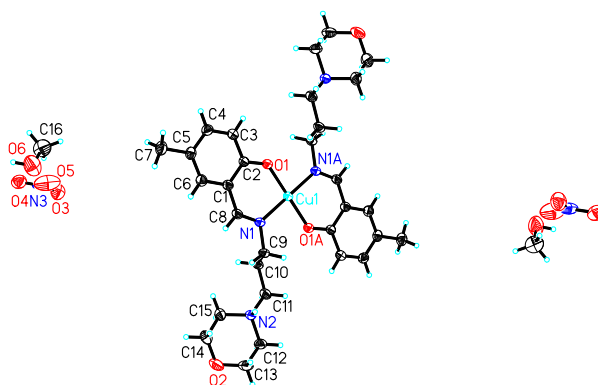


Figure 2. Molecular structure of **2**, showing the atom-numbering scheme. Displacement ellipsoids are drawn at the 30% probability level and H atoms are shown as small spheres of arbitrary radii. Unlabeled atoms or atoms labeled with the suffix A are related to the symmetry position  $-x, -y, -z$ .

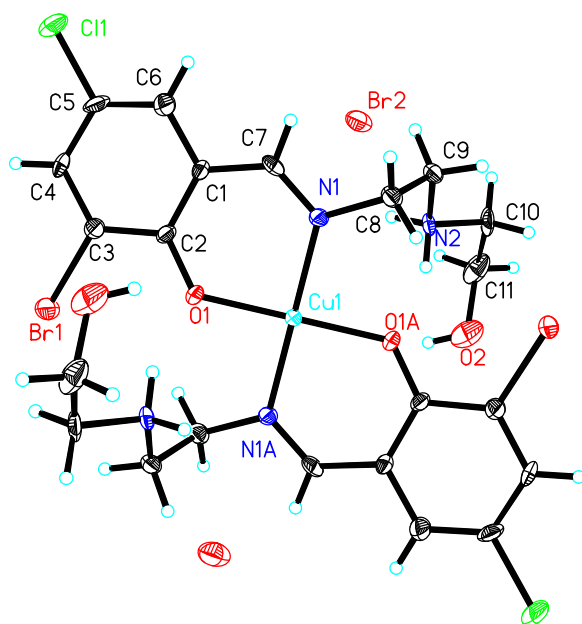


Figure 3. Molecular structure of **3**, showing the atom-numbering scheme. Displacement ellipsoids are drawn at the 30% probability level and H atoms are shown as small spheres of arbitrary radii. Unlabeled atoms or atoms labeled with the suffix A are related to the symmetry position  $-x, 1-y, -z$ .

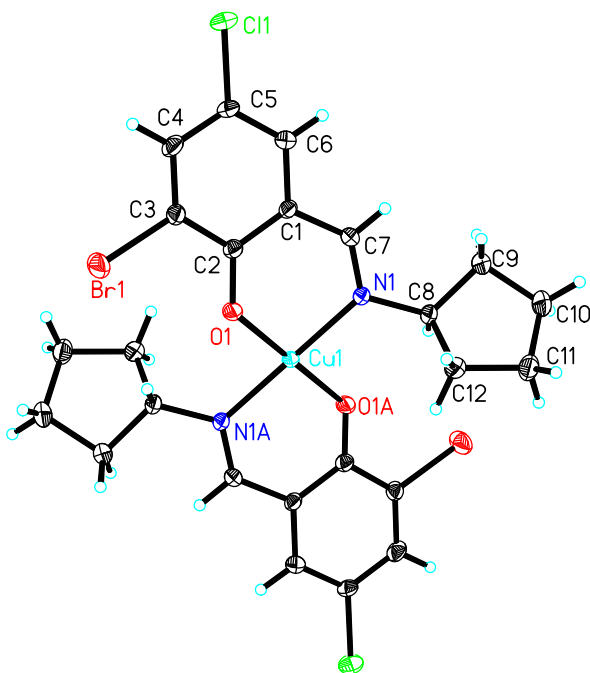


Figure 4. Molecular structure of **4**, showing the atom-numbering scheme.

Displacement ellipsoids are drawn at the 30% probability level and H atoms are shown as small spheres of arbitrary radii. Unlabeled atoms or atoms labeled with the suffix A are related to the symmetry position  $-x, -y, 2-z$ .

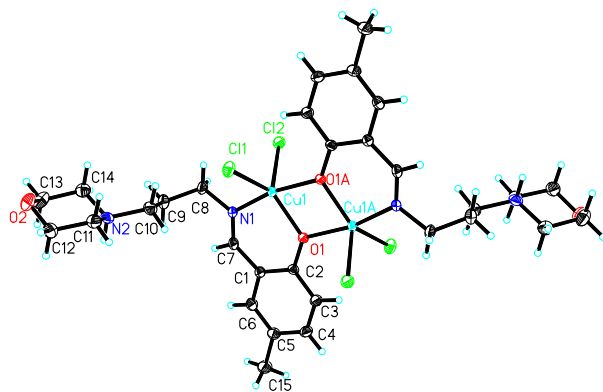


Figure 5. Molecular structure of **5**, showing the atom-numbering scheme. Displacement ellipsoids are drawn at the 30% probability level and H atoms are shown as small spheres of arbitrary radii. Unlabeled atoms or atoms labeled with the suffix A are related to the symmetry position  $2-x, -y, 1-z$ .

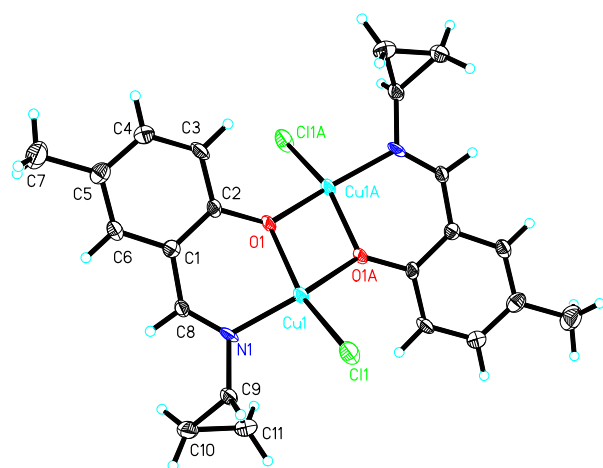


Figure 6. Molecular structure of **6**, showing the atom-numbering scheme. Displacement ellipsoids are drawn at the 30% probability level and H atoms are shown as small spheres of arbitrary radii. Unlabeled atoms or atoms labeled with the suffix A are related to the symmetry position  $2-x, 1-y, 1-z$ .

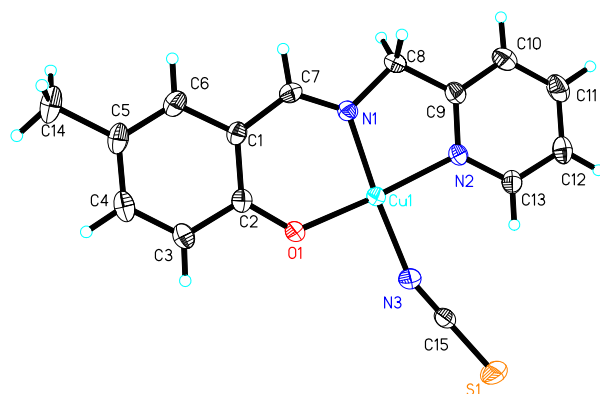


Figure 7. Molecular structure of **7**, showing the atom-numbering scheme. Displacement ellipsoids are drawn at the 30% probability level and H atoms are shown as small spheres of arbitrary radii.

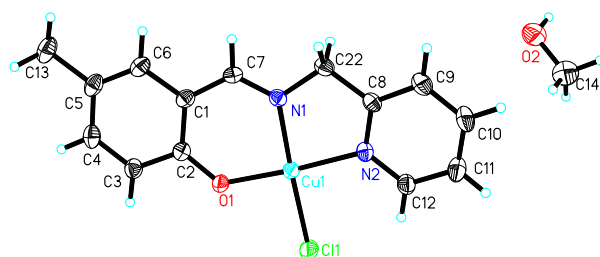


Figure 8. Molecular structure of **8**, showing the atom-numbering scheme. Displacement ellipsoids are drawn at the 30% probability level and H atoms are shown as small spheres of arbitrary radii.

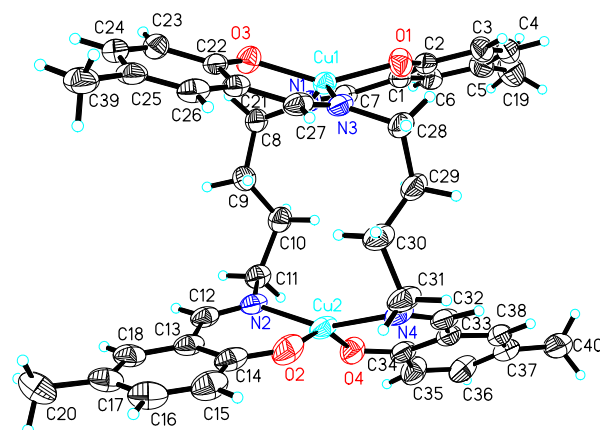


Figure 9. Molecular structure of **9**, showing the atom-numbering scheme. Displacement ellipsoids are drawn at the 30% probability level and H atoms are shown as small spheres of arbitrary radii.

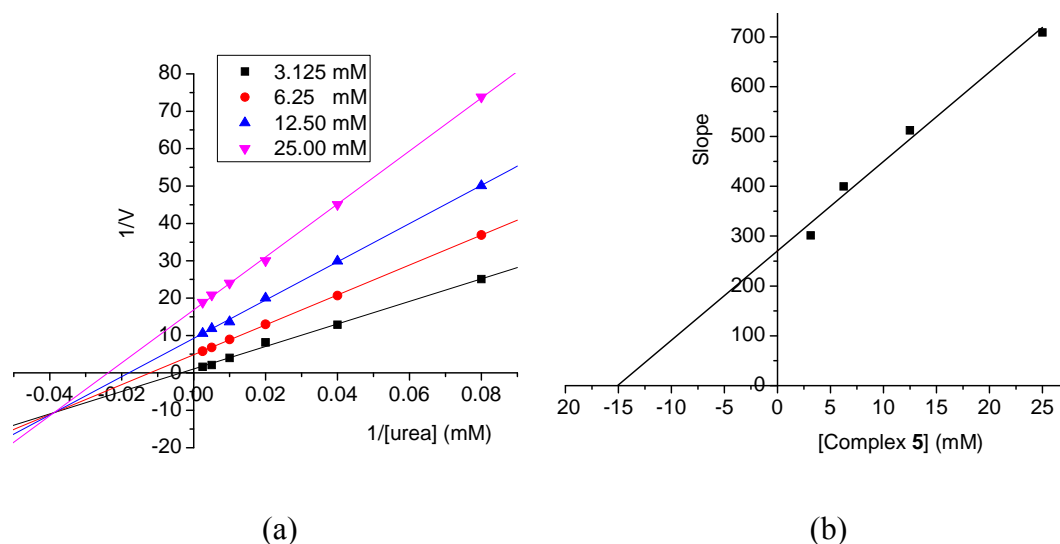


Figure 10. (a) Lineweaver–Burk plot of the reciprocal of initial velocities vs. the reciprocal of substrate concentration in the presence of 25.00, 12.50, 6.25, and 3.125 mM of complex **5**. (b) Plot of the slopes from the Lineweaver-Burk plots vs. various concentrations of complex **5**.

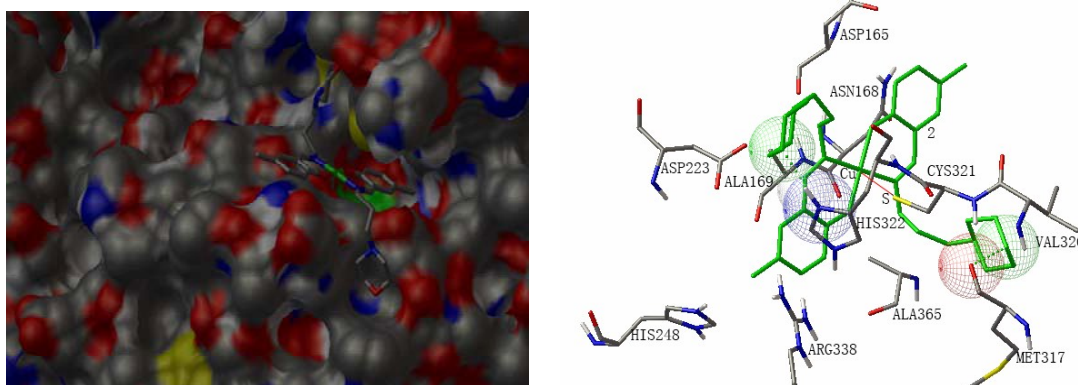


Figure 11. Binding mode of **2** with *Helicobacter pylori* urease. Left: The enzyme is shown as surface, and the complex is shown as sticks. Right: The residues of the enzyme are shown as sticks, and the complex is shown as green lines.

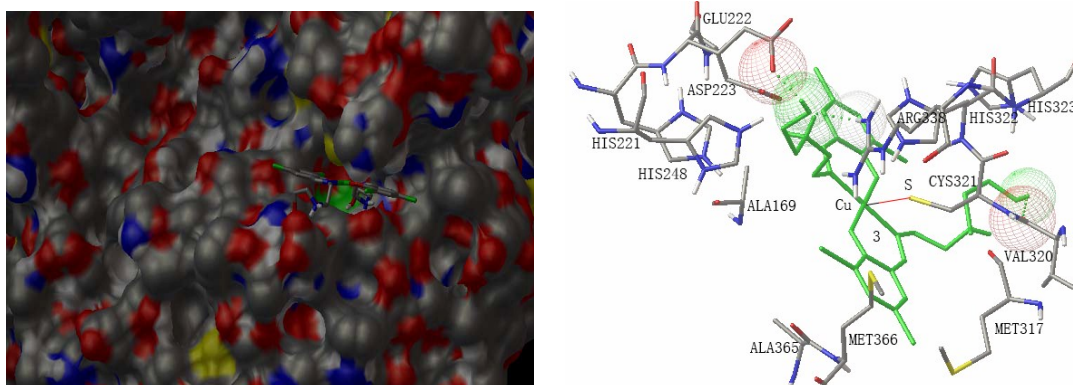


Figure 12. Binding mode of **3** with *Helicobacter pylori* urease. Left: The enzyme is shown as surface, and the complex is shown as sticks. Right: The residues of the enzyme are shown as sticks, and the complex is shown as green lines.

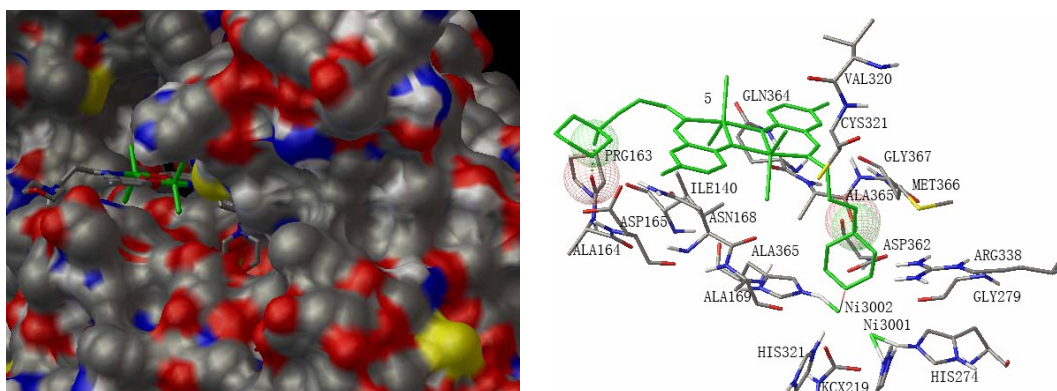


Figure 13. Binding mode of **5** with *Helicobacter pylori* urease. Left: The enzyme is shown as surface, and the complex is shown as sticks. Right: The residues of the enzyme are shown as sticks, and the complex is shown as green lines.

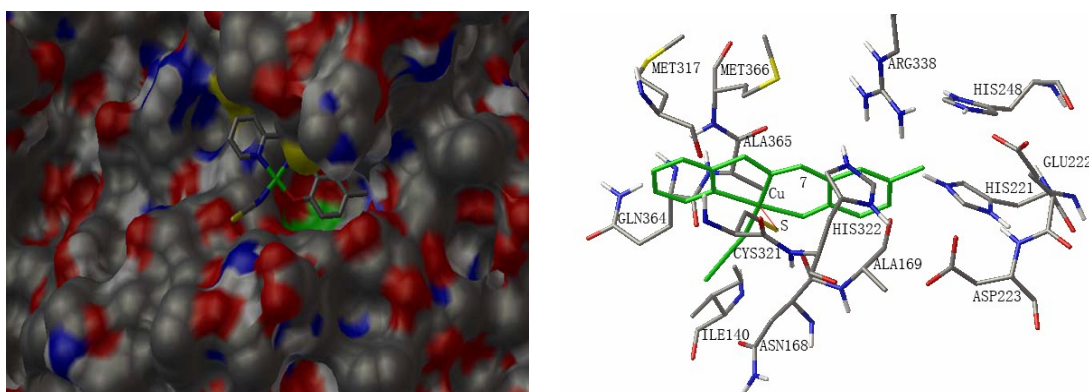


Figure 14. Binding mode of **7** with *Helicobacter pylori* urease. Left: The enzyme is shown as surface, and the complex is shown as sticks. Right: The residues of the enzyme are shown as sticks, and the complex is shown as green lines.

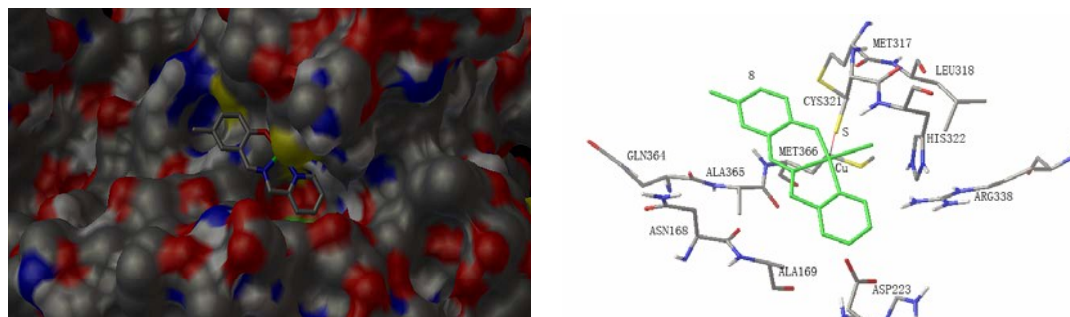


Figure 15. Binding mode of **8** with *Helicobacter pylori* urease. Left: The enzyme is shown as surface, and the complex is shown as sticks. Right: The residues of the enzyme are shown as sticks, and the complex is shown as green lines.

**Table 1a** Crystal data for complexes **1**, **2** and **3**

	<b>1</b>	<b>2</b>	<b>3</b>
Formula	C <sub>36</sub> H <sub>38</sub> Br <sub>2</sub> Cl <sub>2</sub> Cu <sub>2</sub> N <sub>6</sub> O <sub>4</sub>	C <sub>32</sub> H <sub>52</sub> CuN <sub>6</sub> O <sub>12</sub>	C <sub>22</sub> H <sub>28</sub> Br <sub>4</sub> Cl <sub>2</sub> CuN <sub>4</sub> O <sub>4</sub>
FW	976.5	776.3	866.6
Crystal shape/colour	block/blue	block/blue	block/blue
Crystal size /mm	0.27×0.23×0.23	0.26×0.23×0.22	0.19×0.18×0.18
Crystal system	Monoclinic	Monoclinic	Monoclinic
Space group	<i>P</i> 2 <sub>1</sub> / <i>n</i>	<i>P</i> 2 <sub>1</sub> / <i>n</i>	<i>P</i> 2 <sub>1</sub> / <i>c</i>
<i>a</i> (Å)	6.9700(6)	6.7015(4)	7.7486(8)
<i>b</i> (Å)	16.178(1)	15.2568(9)	23.271(3)
<i>c</i> (Å)	17.025(1)	17.924(1)	8.115(1)
<i>α</i> (°)	90	90	90
<i>β</i> (°)	97.144(1)	94.912(2)	94.35(1)

$\gamma(^{\circ})$	90	90	90
$V(\text{\AA}^3)$	1904.9(3)	1825.93(19)	1433.6(1)
$Z$	2	2	2
$\lambda(\text{MoK}\alpha)(\text{\AA})$	0.71073	0.71073	0.71073
$T(\text{K})$	298(2)	298(2)	298(2)
$\mu(\text{MoK}\alpha)(\text{cm}^{-1})$	3.402	0.667	6.445
$T_{\text{min}}$	0.4603	0.8457	0.3740
$T_{\text{max}}$	0.5084	0.8672	0.3900
Reflections/parameters	9904/240	15050/240	6417/170
Unique reflections	3552	3384	2642
Observed reflections [ $I \geq 2\sigma(I)$ ]	3075	2678	1832
Restraints	1	2	0
Goodness of fit on $F^2$	1.024	1.051	1.037
$R_1, wR_2 [I \geq 2\sigma(I)]$	0.0295, 0.0727	0.0428, 0.1053	0.0905, 0.2155
$R_1, wR_2$ (all data)	0.0369, 0.0771	0.0587, 0.1161	0.1221, 0.2417

**Table 1b** Crystal data for complexes **4**, **5** and **6**

	<b>4</b>	<b>5</b>	<b>6</b>
Formula	$\text{C}_{24}\text{H}_{24}\text{Br}_2\text{Cl}_2\text{CuN}_2\text{O}_2$	$\text{C}_{30}\text{H}_{44}\text{Cl}_4\text{N}_2\text{Cu}_2\text{N}_4\text{O}_4$	$\text{C}_{22}\text{H}_{24}\text{Cl}_2\text{Cu}_2\text{N}_2\text{O}_2$
FW	666.7	793.6	546.4
Crystal shape/colour	block/blue	block/blue	block/blue
Crystal size /mm	0.25×0.23×0.22	0.33×0.30×0.27	0.17×0.13×0.13
Crystal system	Monoclinic	Monoclinic	Monoclinic

Space group	<i>P2<sub>1</sub>/c</i>	<i>P2<sub>1</sub>/c</i>	<i>P2<sub>1</sub>/c</i>
<i>a</i> (Å)	9.2353(8)	11.188(2)	7.840(2)
<i>b</i> (Å)	12.4758(6)	16.085(3)	10.704(3)
<i>c</i> (Å)	11.1404(9)	10.081(2)	13.449(2)
$\alpha$ (°)	90	90	90
$\beta$ (°)	109.349(3)	115.675(2)	93.458(3)
$\gamma$ (°)	90	90	90
<i>V</i> (Å <sup>3</sup> )	1211.1(2)	1635.1(5)	1126.6(5)
<i>Z</i>	2	2	2
$\lambda$ (MoK $\alpha$ ) (Å)	0.71073	0.71073	0.71073
<i>T</i> (K)	298(2)	298(2)	298(2)
$\mu$ (MoK $\alpha$ ) (cm <sup>-1</sup> )	4.447	1.670	2.146
<i>T</i> <sub>min</sub>	0.4027	0.6087	0.7118
<i>T</i> <sub>max</sub>	0.4412	0.6613	0.7678
Reflections/parameters	5409/151	8519/204	7719/137
Unique reflections	2255	3043	1922
Observed reflections [ <i>I</i> $\geq 2\sigma(I)$ ]	1672	2406	1599
Restraints	0	1	0
Goodness of fit on <i>F</i> <sup>2</sup>	1.025	1.023	1.052
<i>R</i> <sub>1</sub> , <i>wR</i> <sub>2</sub> [ <i>I</i> $\geq 2\sigma(I)$ ]	0.0338, 0.0733	0.0353, 0.0778	0.0759, 0.2137
<i>R</i> <sub>1</sub> , <i>wR</i> <sub>2</sub> (all data)	0.0536, 0.0824	0.0506, 0.0836	0.0878, 0.2235

**Table 1c** Crystal data for complexes **7**, **8** and **9**

	7	8	9
Formula	C <sub>15</sub> H <sub>13</sub> CuN <sub>3</sub> OS	C <sub>15</sub> H <sub>17</sub> ClCuN <sub>2</sub> O <sub>2</sub>	C <sub>40</sub> H <sub>44</sub> Cu <sub>2</sub> N <sub>4</sub> O <sub>4</sub>
FW	346.9	356.3	771.9
Crystal shape/colour	block/blue	block/blue	block/blue
Crystal size /mm	0.20×0.20×0.20	0.25×0.23×0.23	0.17×0.13×0.13
Crystal system	Monoclinic	Triclinic	Monoclinic
Space group	<i>P</i> 2 <sub>1</sub> / <i>n</i>	<i>P</i> -1	<i>P</i> 2 <sub>1</sub> / <i>c</i>
<i>a</i> (Å)	6.9863(4)	7.2905(8)	24.219(3)
<i>b</i> (Å)	15.3790(8)	9.092(1)	10.240(1)
<i>c</i> (Å)	13.3498(8)	11.812(1)	15.679(2)
$\alpha$ (°)	90	100.605(3)	90
$\beta$ (°)	91.874(2)	98.485(3)	107.360(2)
$\gamma$ (°)	90	91.807(3)	90
<i>V</i> (Å <sup>3</sup> )	1433.6(1)	759.8(1)	3711.3(8)
<i>Z</i>	4	2	4
$\lambda$ (MoK $\alpha$ ) (Å)	0.71073	0.71073	0.71073
<i>T</i> (K)	298(2)	298(2)	298(2)
$\mu$ (MoK $\alpha$ ) (cm <sup>-1</sup> )	1.607	1.618	2.146
<i>T</i> <sub>min</sub>	0.7312	0.6879	0.7163
<i>T</i> <sub>max</sub>	0.7312	0.7073	0.7391
Reflections/parameters	14017/191	6463/193	19090/454
Unique reflections	3268	2760	6919
Observed reflections [ <i>I</i> ≥ 2 $\sigma$ ( <i>I</i> )]	2700	2490	4647

---

Restraints	0	0	0
Goodness of fit on $F^2$	1.100	1.074	1.006
$R_1, wR_2 [I \geq 2\sigma(I)]$	0.0352, 0.0797	0.0417, 0.1010	0.0355, 0.0798
$R_1, wR_2$ (all data)	0.0487, 0.0860	0.0478, 0.1061	0.0655, 0.0933

---

**Table 2** Selected bond lengths (Å) and angles (°) for the complexes

<b>1</b>			
Cu1-O1	1.938(2)	Cu1-N1	1.939(2)
Cu1-O1A	1.970(2)	Cu1-O2	1.976(2)
Cu1-Br1	2.6678(5)		
O1-Cu1-N1	90.85(8)	O1-Cu1-O1A	79.57(8)
N1-Cu1-O1A	155.60(9)	O1-Cu1-O2	167.51(9)
N1-Cu1-O2	80.86(8)	O1-Cu1-O2A	104.31(7)
O1-Cu1-Br1	96.57(7)	N1-Cu1-Br1	104.37(7)
O1-Cu1-Br1A	99.02(7)	O2-Cu1-Br1A	94.55(6)
<b>2</b>			
Cu1-O1	1.896(2)	Cu1-N1	2.005(2)
O1-Cu1-O1A	180	O1-Cu1-N1A	88.25(8)
O1-Cu1-N1	91.75(8)	N1-Cu1-N1A	180
<b>3</b>			
Cu1-O1	1.935(7)	Cu1-N1	2.010(7)
O1-Cu1-O1A	180	O1-Cu1-N1A	88.6(3)
O1-Cu1-N1	91.4(3)	N1-Cu1-N1A	180
<b>4</b>			
Cu1-O1	1.905(2)	Cu1-N1	2.018(2)
O1-Cu1-O1A	180	O1-Cu1-N1A	89.4(1)
O1-Cu1-N1	90.6(1)	N1-Cu1-N1A	180
<b>5</b>			
Cu1-N1	1.968(2)	Cu1-O1	2.008(2)
Cu1-Cl1	2.3075(9)	Cu1-Cl2	2.5072(9)

N1-Cu1-O1A	167.73(9)	N1-Cu1-O1	92.16(9)
O1-Cu1-O1A	75.91(9)	N1-Cu1-Cl1	93.26(8)
O1-Cu1-Cl1A	97.18(6)	O1-Cu1-Cl1	134.56(7)
N1-Cu1-Cl2	87.83(8)	O1-Cu1-Cl2A	95.15(7)
O1-Cu1-Cl2	117.83(7)	Cl1-Cu1-Cl2	107.43(3)
<b>6</b>			
Cu1-Cl1	2.198(2)	Cu1-O1	1.933(5)
Cu1-N1	1.947(6)	Cu1-O1A	1.964(5)
O1-Cu1-N1	94.2(2)	O1-Cu1-O1A	76.3(2)
N1-Cu1-O1A	152.1(3)	O1-Cu1-Cl1	150.7(2)
N1-Cu1-Cl1	98.7(2)	O1-Cu1-Cl1A	102.2(2)
<b>7</b>			
Cu1-O1	1.903(2)	Cu1-N1	1.926(2)
Cu1-N2	2.022(2)	Cu1-N3	1.929(2)
O1-Cu1-N1	93.78(7)	O1-Cu1-N3	90.12(8)
N1-Cu1-N3	176.10(9)	O1-Cu1-N2	176.40(7)
N1-Cu1-N2	82.68(8)	N3-Cu1-N2	93.42(9)
<b>8</b>			
Cu1-O1	1.900(2)	Cu1-N1	1.947(3)
Cu1-N2	2.008(3)	Cu1-Cl1	2.233(1)
O1-Cu1-N1	92.8(1)	O1-Cu1-N2	173.8(1)
N1-Cu1-N2	82.5(1)	O1-Cu1-Cl1	89.21(8)
N1-Cu1-Cl1	177.38(9)	N2-Cu1-Cl1	95.58(9)
<b>9</b>			
Cu1-O1	1.887(2)	Cu1-O3	1.887(2)

Cu1-N3	1.972(2)	Cu1-N1	1.972(2)
Cu2-O2	1.881(3)	Cu2-O4	1.888(2)
Cu2-N2	1.967(2)	Cu2-N4	1.971(3)
O1-Cu1-O3	148.51(9)	O1-Cu1-N3	93.0(1)
O3-Cu1-N3	94.89(9)	O1-Cu1-N1	94.34(9)
O3-Cu1-N1	92.48(9)	N3-Cu1-N1	152.60(9)
O2-Cu2-O4	147.0(1)	O2-Cu2-N2	93.9(1)
O4-Cu2-N2	92.9(1)	O2-Cu2-N4	93.4(1)
O4-Cu2-N4	94.4(1)	N2-Cu2-N4	154.0(1)

**Table 3** Hydrogen bond distances (Å) and bond angles (°) for the complexes

$D-H\cdots A$	$d(D-H)$	$d(H\cdots A)$	$d(D\cdots A)$	Angle ( $D-H\cdots A$ )
<b>1</b>				
N2-H2 $\cdots$ Br1 <sup>i</sup>	0.90(1)	2.43(1)	3.317(2)	168(4)
<b>2</b>				
N2-H2 $\cdots$ O3 <sup>ii</sup>	0.90(1)	2.09(2)	2.862(4)	143(3)
N2-H2 $\cdots$ O4 <sup>ii</sup>	0.90(1)	2.21(2)	3.061(4)	158(3)
N2-H2 $\cdots$ N3 <sup>ii</sup>	0.90(1)	2.54(1)	3.434(4)	170(3)
O6-H6 $\cdots$ O3 <sup>iii</sup>	0.91(1)	1.95(2)	2.824(5)	161(4)
<b>3</b>				
N2-H2B $\cdots$ Br1 <sup>iv</sup>	0.90	3.10	3.626(9)	120
N2-H2B $\cdots$ O1 <sup>iv</sup>	0.90	1.97	2.82(1)	156
O2-H2 $\cdots$ Br2 <sup>v</sup>	0.82	2.58	3.33(1)	151
N2-H2A $\cdots$ Br2 <sup>v</sup>	0.90	2.80	3.417(8)	127
N2-H2A $\cdots$ Br2	0.90	2.70	3.377(8)	132

<b>5</b>				
N2–H2...Cl2 <sup>vi</sup>	0.90(1)	2.38(2)	3.164(3)	145(3)
N2–H2...Cl2 <sup>vii</sup>	0.90(1)	2.82(3)	3.445(3)	127(3)
<b>8</b>				
O2–H2...Cl1 <sup>viii</sup>	0.82	2.95	3.624(4)	141
O2–H2...O1 <sup>viii</sup>	0.82	2.15	2.892(4)	151

Symmetry codes: (i)  $1 + x, y, z$ ; (ii)  $x, -1 + y, z$ ; (iii)  $1 + x, y, z$ ; (iv)  $-x, 1 - y, -z$ ; (v)  $-x, 1 - y, 1 - z$ ; (vi)  $2 - x, 1/2 + y, 3/2 - z$ ; (vii)  $x, 1/2 - y, -1/2 + z$ ; (viii)  $-1 + x, -1 + y, z$ .

**Table 4** Inhibition of urease by the tested materials

Tested materials	Percentage Inhibition rate <sup>#</sup>	IC <sub>50</sub> (μM)
<b>1</b>	32.0 ± 2.1	> 100
<b>2</b>	88.3 ± 3.7	0.37 ± 1.22
<b>3</b>	82.5 ± 4.0	0.21 ± 0.97
<b>4</b>	56.9 ± 2.6	80.1 ± 3.2
<b>5</b>	80.7 ± 3.1	0.03 ± 0.78
<b>6</b>	44.5 ± 4.3	> 100
<b>7</b>	90.2 ± 2.9	0.39 ± 0.58
<b>8</b>	90.3 ± 3.7	0.76 ± 0.95
<b>9</b>	22.9 ± 1.8	> 100
Copper perchlorate	87.5 ± 2.6	8.8 ± 1.4
Acetohydroxamic acid	84.3 ± 3.9	37.2 ± 4.0
Ref. [39]	–	0.46 and 0.52
Ref. [47]	–	35

---

Ref. [48]	–	19 and 39
Ref. [49]	–	4.71 and 3.15
Ref. [50]	–	4.052 and 6.868
Ref. [51]	–	1.17 – 35.7
Ref. [52]	–	1.45 – 3.22

---

<sup>#</sup>The concentration of the tested material is 100  $\mu\text{M}$ .

## Graphical Abstract

**Nine new copper(II) complexes derived from various Schiff bases were prepared. Five complexes show effective urease inhibitory activities. Complex 5 has the most effective activity against urease, with a mixed competitive inhibition mechanism.**

